# Electronic States at Low-Angle Grain Boundaries in Polycrystalline Naphthalene

Marko Mladenović,[*,†,‡] Nenad Vukmirović,[†] and Igor Stanković[†]

[†]Scientific Computing Laboratory, Institute of Physics Belgrade, University of Belgrade, Pregrevica 118, 11080 Belgrade, Serbia
[‡]School of Electrical Engineering, University of Belgrade, P.O. Box 35-54, 11120 Belgrade, Serbia

ABSTRACT: We investigated the influence of grain boundaries on electronic properties of polycrystalline organic semiconductor naphthalene. The atomic structure of grain boundaries was found using a Monte Carlo method, whereas electronic structure calculations were performed using the charge patching method. We found that grain boundaries introduce trap states within the band gap of the material. Our results show that spatial positions and energies of trap states can be predicted solely from geometrical arrangement of molecules near the boundary. Wave functions of these states are localized on closely spaced pairs of molecules from opposite sides of the boundary. The energies of trap states are strongly correlated with the distances between the molecules in the pair. These findings were used to calculate the electronic density of trap states, which was found to exhibit a qualitatively different behavior for grain boundaries perpendicular to the a and b directions of the crystal unit cell.
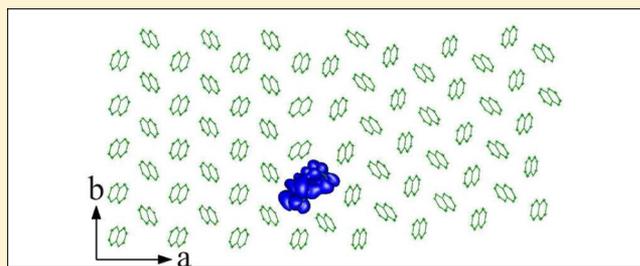
INTRODUCTION

Organic semiconductors are materials of great promise for electronic devices, such as organic field-effect transistors (FETs), organic light-emitting diodes (LEDs), and organic solar cells (OSCs).[1–7] Their advantage over inorganic counterparts is that they are flexible and have a low processing cost. However, devices made of organic semiconductors still have relatively low charge mobility and low efficiency. Small molecule based crystalline organic semiconductors (such as tetracene, pentacene, rubrene, etc.) exhibit the highest mobilities among organic semiconductors due to their crystalline structures. Electronic devices based on these materials are typically obtained using the vacuum-evaporation technique.[8–13] More recently, it became possible to use an inexpensive solution processing technique to obtain structures with a high degree of crystallinity and good charge transport properties,[14–19] which opens the way toward large-scale applications of small molecule based organic semiconductors. Therefore, researchers put effort into improving properties of these materials in order to make them competitive with inorganic semiconductors.

Thin films of crystalline organic semiconductors have a polycrystalline form, which is composed of many different crystalline grains. It has been shown that the transport in a single grain boundary device is limited by the grain boundary.[9] A pronounced dependence of transistor characteristics on the grain size was also established,[12,15,16,20] as well as a strong difference between the characteristics of single-crystal and polycrystalline transistors based on the same material.[11] It was also shown that grain boundary orientation has a large influence on the charge carrier mobility.[18] All of these results indicate that grain boundaries are the most limiting intrinsic factor for efficient charge transport in small molecule based polycrystalline organic semiconductors.

However, there is still a lack of understanding of the specific mechanism by which grain boundaries affect the charge transport. It is typically assumed that they introduce trap states localized at the grain boundary, with energies of these states within the band gap of the material.[9,11,12,20–22] The charges in the trap states do not contribute to transport, and therefore, the presence of traps reduces the effective charge carrier mobility. On the other hand, there are some suggestions that grain boundaries act as barriers and that charge carriers are trapped in the grains.[23,24] Calculations of electrostatic potential at molecules near the grain boundary formed from two misaligned grains indicate the presence of trapping centers at the boundary.[25] Other theoretical and computational studies are primarily focused on the properties of single crystals.[26–37]

In this paper, we shed light on the nature of electronic states at grain boundaries in organic crystalline semiconductors. We directly calculate the wave functions of electronic states and gain microscopic insight into the origin of these states. Using these insights, we develop a simple model for density of trap states prediction. In the following section, the method for electronic structure calculation is introduced. We use naphthalene as a representative of crystalline organic semiconductors based on small molecules. The results of the calculation of electronic states at grain boundaries are

presented. We find that grain boundaries produce trap states in the band gap, where the highest states are localized on pairs of molecules at the grain boundary, whose mutual distance is much smaller than the corresponding distance in the monocrystal. Strong correlation between the mutual distance between these molecules and the energies of these states was found. Such a correlation enables one to calculate the electronic density of states at the grain boundary directly from mutual distances between molecules. Finally, the results obtained are discussed with a particular focus on their relation to the current body of knowledge about grain boundaries in organic polycrystals.

■ METHOD FOR ELECTRONIC STRUCTURE CALCULATIONS

The method used for electronic structure calculations of grain boundaries in polycrystalline naphthalene is schematically described in Figure 1. The atomic structure is obtained from
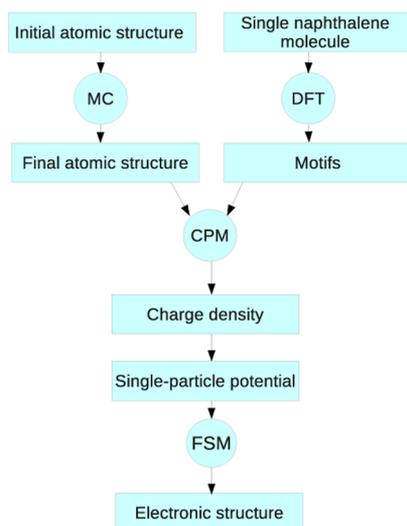

Figure 1. Schematic representation of the algorithm for electronic structure calculations.

a relaxation procedure based on a Monte Carlo (MC) method[38] and is subsequently used to calculate the electronic states using the density functional theory (DFT)[39] based charge patching method (CPM).[40,41]

The initial configuration for MC relaxation is two monocrystals with different crystalline orientations joined at their common boundary. Potential energy of a system is calculated using transferable potentials for phase equilibria (TraPPE).[42,43] Naphthalene molecules are considered as rigid bodies; hence, only interactions between carbon atoms from different molecules described by the weak van der Waals interaction are taken into account. Carbon-hydrogen (CH) groups are treated as one atom with a center of mass at carbon atoms. TraPPE parameters for interactions between CH groups are $\sigma = 3.695$ Å, $\varepsilon/k_B = 50.5$ K and, for interaction between C atoms, $\sigma = 3.7$ Å, $\varepsilon/k_B = 30$ K. An MC algorithm was then used to minimize the energy of the system. In each step of the MC algorithm, one molecule is randomly chosen, translated for a randomly chosen vector, and rotated by a randomly chosen angle. The decision about the acceptance of this move is made according to the Metropolis algorithm: if the energy of the new configuration is lower than the initial, the move is accepted;

otherwise, it is accepted with a probability equal to the Boltzmann weight of the difference of the energy of the new and the old configuration.[38] The simulation is performed until a thermal equilibrium is reached, which is evidenced by the saturation in the dependence of the energy on the number of simulation steps. Simulation is performed at a temperature of 300 K. After the thermal equilibrium is reached, the system is gradually cooled down to 0 K. In this way, dynamic disorder (crystal disorder induced by thermal motion) effects[26] are excluded. Both the effects of dynamic disorder and grain boundaries can, in principle, induce localized states, and it would be very difficult to distinguish between these if the electronic structure calculations were performed for a structure obtained from a snapshot of MC simulations at 300 K. To check that the choice of the temperature of 300 K has only a small effect on the final atomic structure obtained from an MC procedure, we repeated the simulations using the temperatures of 100, 200, and 400 K, as well. Atomic structures obtained from these simulations were nearly identical as the atomic structure obtained from the simulation at 300 K. Therefore, the MC simulation procedure is robust in the sense that the final structure is weakly dependent on the details of the procedure.

TraPPE empirical potentials were previously used for a variety of organic materials.[43−45] The validity of the potentials used in the MC simulation was verified by comparing the naphthalene crystal lattice constants obtained from these empirical potentials to the values from the literature. The initial structure for the crystal lattice parameters optimization is the naphthalene unit cell with the lattice parameters and atomic structure given in ref 46. It is assumed that two angles of the unit cell are 90°, since the naphthalene unit cell is monoclinic.[47] Other unit cell parameters (three lengths and one angle) were varied and MC relaxation was performed for each combination of the unit cell parameters until the convergence of the potential energy was satisfied. In the same manner as for the atomic structure of grain boundaries, the simulation was first performed at 300 K, followed by gradually cooling down to 0 K. The obtained lattice constants are constants that give the crystal lattice with minimal potential energy: $a = 8.325$ Å, $b = 5.92$ Å, $c = 7.77$ Å, and $\beta = 63°$. In the literature, there are several results for naphthalene unit cell parameters: In ref 48: $a = 8.4$ Å, $b = 6$ Å, $c = 8.66$ Å, and $\beta = 57.1°$. In ref 49: $a = 8.098$ Å, $b = 5.953$ Å, $c = 8.652$ Å, and $\beta = 55.6°$. Therefore, lattice constants obtained with TraPPE empirical potentials are in good agreement with previous results. Simulations were performed using temperatures other than 300 K, as well, to check the correctness of the procedure and the results. For additional evaluation of the validity of empirical potentials, the melting temperature of naphthalene was calculated as the temperature of the heat capacity peak.[50] The calculated melting temperature is 340 ± 5 K, which is close to the melting temperature of 352.5 K given in ref 51.

After the atomic structure is obtained, electronic structure calculations can be performed. In principle, DFT can be used for that. However, to avoid finite size effects on the electronic states at the grain boundaries, one needs to include a sufficiently large number of unit cells in the plane of the boundary, as well as several molecular layers nearest to the boundary. This typically includes several thousand atoms, which is beyond the reach of standard DFT calculations. Therefore, the CPM was used instead of standard DFT. CPM is a strong tool by which one can directly construct the electronic charge density instead of self-consistently solving the

Kohn–Sham equations as in standard calculations based on DFT. In the CPM, an appropriate motif is assigned to each atom in the system. Motif is a description of the environment of an atom. It contains the information about the types of the central atom and its neighbors. There are five motifs in the system that consists of naphthalene molecules only: C_3–$C_3C_2C_2$, C_2–C_3C_2H, C_2–C_2C_2H, H–C_2–C_2C_2, and H–C_2–C_3C_2, where C_X is the carbon atom connected to X other carbon atoms. Charge density of a motif associated with an atom A is calculated using the formula

$$m_A(\mathbf{r} - \mathbf{R}_A) = \frac{w_A(\mathbf{r} - \mathbf{R}_A)}{\sum_B w_B(\mathbf{r} - \mathbf{R}_B)} \rho(\mathbf{r}) \tag{1}$$

where $\rho(\mathbf{r})$ is the charge density of a single naphthalene molecule obtained by DFT calculations, while $\mathbf{R}_A$ and w_A are, respectively, the position and the weight function of the atom A. Overall charge density is then calculated as a sum of all motif charge densities in the system. With charge density at hand, the single-particle Hamiltonian is given as

$$H = -\frac{\hbar^2}{2m_0}\nabla^2 + v_I + \frac{e}{4\pi\varepsilon_0}\int \frac{\rho(\mathbf{r}')}{|\mathbf{r} - \mathbf{r}'|}d\mathbf{r}' + v_{xc}^{LDA}(\rho) \tag{2}$$

The first term in eq 2 is the kinetic energy, the second term is the atomic core pseudopotential modeled using norm-conserving pseudopotentials, the third term is the electrostatic Hartree potential, while the fourth term is the exchange-correlation term, which is modeled using the local density approximation (LDA). The eigenvalue problem of the Hamiltionian is solved using the folded spectrum method (FSM),[52] as implemented in the PESCAN code that gives the electronic states around the desired energy, which is the top of the valence band in our case.

■ WAVE FUNCTIONS AT GRAIN BOUNDARIES

In this section, the wave functions of states at grain boundaries are presented. We consider the system consisting of 1000 molecules (500 at each side of the boundary) arranged in 10 layers that are parallel to the ab plane[47] of the unit cell. Electronic structure calculations are performed for a single layer of molecules, which is sufficient to describe the electronic properties of the material, because the electronic coupling in the c direction is much weaker than that in the ab plane. Calculations are performed for several misorientation angles between the grains: 5, 10, 15, and 20° and for two types of grain boundaries: (1) perpendicular to the a direction (a-boundary) and (2) perpendicular to the b direction (b-boundary) of the unit cell. Only small angles are considered, because the total energy of the system increases as the angle of misorientation increases, as demonstrated in Figure 2. For each system, the energies of the 10 highest occupied states in the valence band and their wave functions are calculated.

Results of electronic structure calculations for the a-boundary system with a misorientation angle of 10° are presented in Figure 3. These results indicate that there are several states in the band gap whose energies are significantly higher than the energies of the other states. These states are trap states for charge carriers and could strongly affect transport properties of the material. Wave functions of the first and the second highest occupied states are localized on the two molecules at the grain boundary. The distance between these two molecules (defined hereafter as the distance between their centers of mass) is 3.45
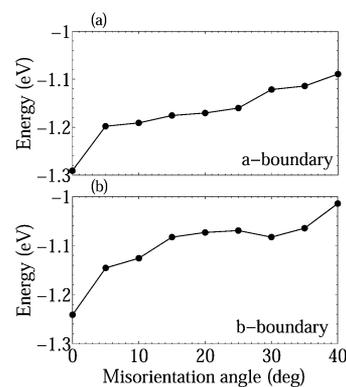

Figure 2. Dependence of potential energy of the system per molecule on the misorientation angle between monocrystal grains for a-boundary systems (a) and b-boundary systems (b). Each system consists of 1000 molecules.
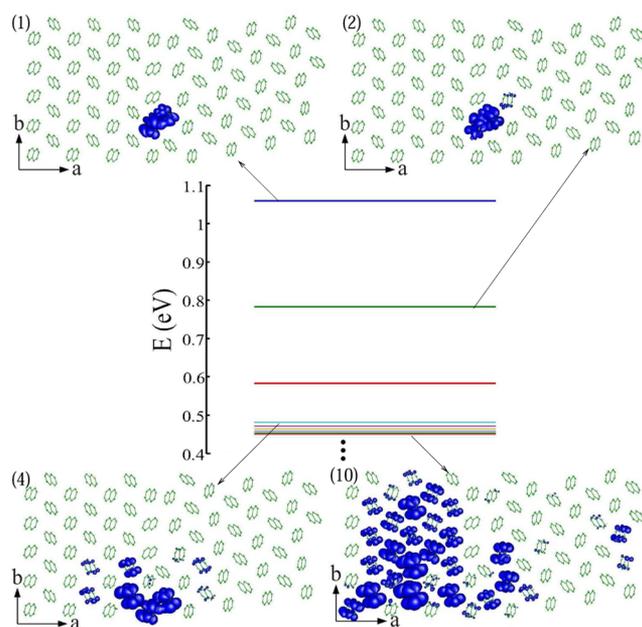

Figure 3. Energies of the states at the top of the valence band and the isosurfaces of their wave function moduli for the system with the misorientation angle of 10° and the grain boundary perpendicular to the a direction. Isosurfaces correspond to the probability of finding a hole inside the surface of 90%.

Å, while the distance between two nearest molecules in the monocrystal is about 5 Å. The highest occupied states in organic semiconductors originate from electronic coupling of the HOMO (highest occupied molecular orbital) levels of different molecules. Electronic coupling that results from the overlap of HOMO orbitals is strongest for closely spaced molecules. As a consequence, the highest state in Figure 3 is localized on two molecules with the smallest mutual distance. It is the bonding states of HOMO orbitals of the two molecules, whereas the second state in Figure 3 is the antibonding state. At certain energies, the spectrum becomes nearly continuous and the states that are completely delocalized start to appear, such as the 10th calculated state; see Figure 3. States like this originate from delocalized Bloch states of the monocrystal and, therefore, are not induced by grain boundaries.

Electronic calculations for other misorientation angles and boundary directions show similar results. In Figure 4, the results
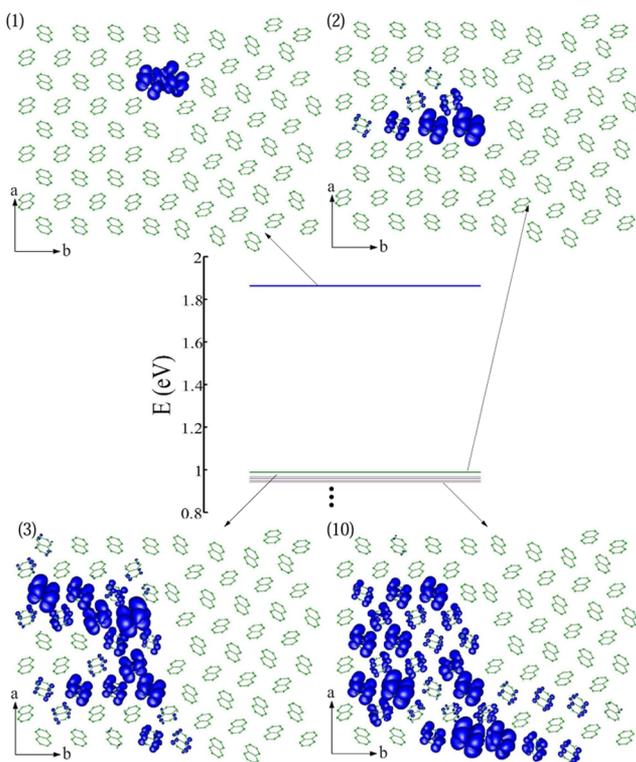
Figure 4. Energies of the states at the top of the valence band and the isosurfaces of their wave function moduli for the system with the misorientation angle of 10° and the grain boundary perpendicular to the *b* direction. Isosurfaces correspond to the probability of finding a hole inside the surface of 90%.
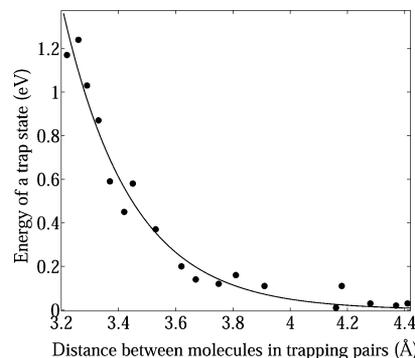

Figure 5. The dependence of the energy of the grain boundary induces trap states on the distance between molecules in trapping pairs. The data obtained from all simulated systems are presented in the figure. Energies of the trapping states are defined with the top of the valence band as a reference level.

for the *b*-boundary system and the misorientation angle of 10° are presented. In this case, there is only one molecule pair at the grain boundary with a small mutual distance and, consequently, one trap state deep in the band gap. Other states are delocalized.

The presented results indicate that grain boundaries introduce electronic states within the band gap of the material. Hereafter, the states localized at the boundaries will be called trap states, whereas delocalized states will be called valence band states. Some trap states are very deep in the band gap, even more than 1 eV above the valence band. As a reference, the experimentally measured band gap of naphthalene is about 5.2 eV.[48] The traps with energies significantly above the top of the valence band (more than 0.1 eV) are always localized on two molecules belonging to different grains with a mutual distance less than the distance between two nearest molecules in the monocrystal. Such pairs of molecules will be hereafter called trapping pairs. Other localized states at the grain boundary have energies very close to the energies of the top of the valence band (second state in Figure 4, for example). Consequently, only pairs of molecules (trapping pairs) will be taken into account. We find that there is a strong correlation between the distance between the molecules in trapping pairs and the energy of the trap electronic states. This dependence is shown in Figure 5. The best fit of this dependence is given by an exponential function $\Delta E = A e^{B(R-R_0)}$, where $A = 1.4064$ eV, $B = -4.181$ Å^{-1}, and $R_0 = 3.2$ Å.

DENSITY OF TRAP STATES AT GRAIN BOUNDARIES

Electronic structure calculations can be performed for relatively small boundaries only. Although such calculations were highly valuable for understanding the origin and the degree of wave function localization at the boundary, they do not provide sufficient statistics to reliably calculate the density of trap states. On the other hand, the remarkable dependence, presented in Figure 5, can be used to predict the energy of a trap at a given boundary without any electronic calculation, solely based on the distances between the molecules. This allows us to calculate the energies of all trap states for very large grain boundaries and, consequently, calculate the electronic density of trap states. On the basis of the degree of scattering of the data from the fit in Figure 5, we estimate that this method produces an error in the trap energy calculation of up to 0.1 eV.

Consequently, we have demonstrated that computationally demanding electronic structure calculations can be avoided using the aforementioned approach. Next, we show that even the MC relaxation step can be avoided without significantly compromising the accuracy of the electronic density of trap states. By inspecting the atomic structure near the boundaries in Figure 3, one can notice that it stays nearly unchanged after the relaxation. Only molecules in the vicinity of the boundary slightly change their positions and orientations. The difference in the distance between two molecules in trapping pairs, before and after the relaxation, is below 0.1 Å, as demonstrated in Figure 6. Consequently, both MC relaxation and electronic structure calculations can be avoided in the calculation of electronic density of trap states.

The electronic density of trap states was extracted from the calculations of grain boundaries that contain 100 000 molecules arranged in 100 layers. In the construction of the grain boundary atomic structure, there is an ambiguity related to the width of the void between the two monocrystals that form the boundary. This issue was overcome by shifting one of the crystals in the direction perpendicular to the boundary and selecting the void width in such a way that the potential energy of the system is minimal. The distribution of distances between trapping pairs of molecules is calculated then. Next, using the previously introduced exponential fitting function, the electronic density of trap states is obtained. The results are presented for four different angles: 5, 10, 15, and 20° and for two orientations of grain boundaries: *a*-boundary and *b*-
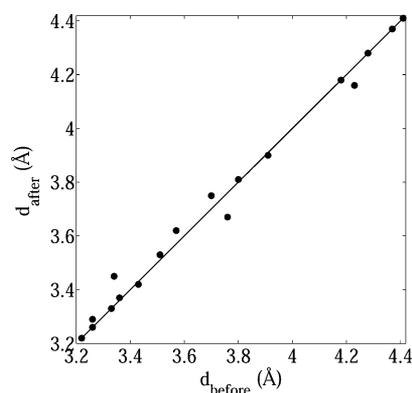
Figure 6. Dependence of the distance between trapping molecule pairs after MC relaxation (d_{after}) on the distance between them before MC relaxation (d_{before}).

boundary. As can be seen from Figure 5, trapping pairs with mutual distances below 4 Å are responsible for traps that are deep in the band gap. Other trapping pairs produce shallow traps that are close to the top of the valence band. The distribution of distances between molecules in trapping pairs at the grain boundaries is shown in Figure 7. One should note that
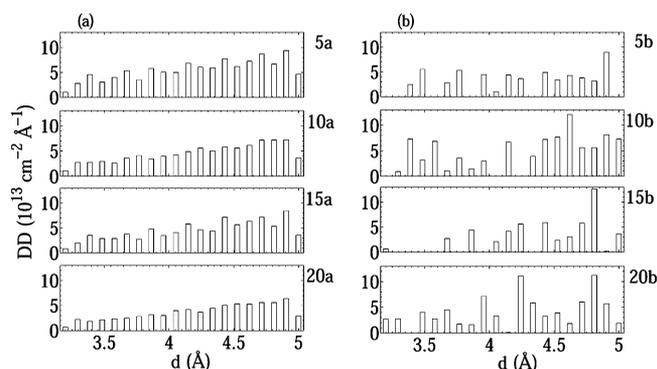

Figure 7. Trapping pair distance (d) distributions (DD) at different grain boundaries. The boundaries are denoted as Xy, where X is the angle between monocrystal grains and y is the direction perpendicular to the boundary surface.

molecule pairs with distances below 3.2 Å can also exist. However, these were not present in small systems calculated in the previous section; hence, their energy cannot be reliably

calculated using the fitting function. Nevertheless, such states are rather rare and we neglect their surface density.

By inspecting Figure 7, one can notice that trapping pair distance distributions for a-boundary systems are similar for all angles. All of them are increasing functions with similar shapes. On the other hand, the distributions for b-boundary systems largely depend on misorientation angle. In addition, the distribution is not continuous as it is for a-boundary and some distances are preferred. This difference can be explained by the geometry of the naphthalene unit cell. Only a and c directions of the unit cell are not perpendicular. Therefore, the c direction is not parallel to the a-boundary surface. For this reason, in the case of a-boundary, different ab planes give different contributions to the trapping pair distance distribution. By adding the contribution from different ab planes, one obtains a continuous function. In the case of b-boundary, the c direction is parallel to the grain boundary surface. Consequently, molecule pairs from one ab plane have their copies in other ab planes and each ab plane gives the same contribution to trapping pair densities. This produces discrete trapping pair distance distributions. The difference between a- and b-boundary is illustrated in Figure 8, where spatial distribution of trapping pair distance is given. Each filled circle in Figure 8 represents a molecule in the layer at the grain boundary. The color of the circle indicates the distance between that molecule and the nearest molecule from the opposite side of the boundary. As one can notice, in the case of a-boundary, distributions for different ab planes are different (as evidenced by the nonperiodicity of the pattern shown in Figure 8a), whereas distributions for different ab planes in the case of b-boundary are equal (as evidenced by the periodic pattern in Figure 8b).

With trapping pair distance distributions at hand, the electronic density of trap states can be straightforwardly calculated as explained. Densities of trap states for eight aforementioned boundaries are given in Figure 9. Because the focus of this work is on trap states that are significantly above the top of the valence band, only trapping pairs with mutual distances below 4 Å are included in the distribution shown in Figure 9. In addition, we have assumed that each trapping pair introduces one trap state, although, in some cases, it can introduce two trap states, as demonstrated in Figure 3. For a-boundary systems, the density of trap states weakly depends on angle. Going deeper in the band gap, the density of trap states monotonously decreases, which is a consequence of the monotonously decreasing density of trapping pairs at the
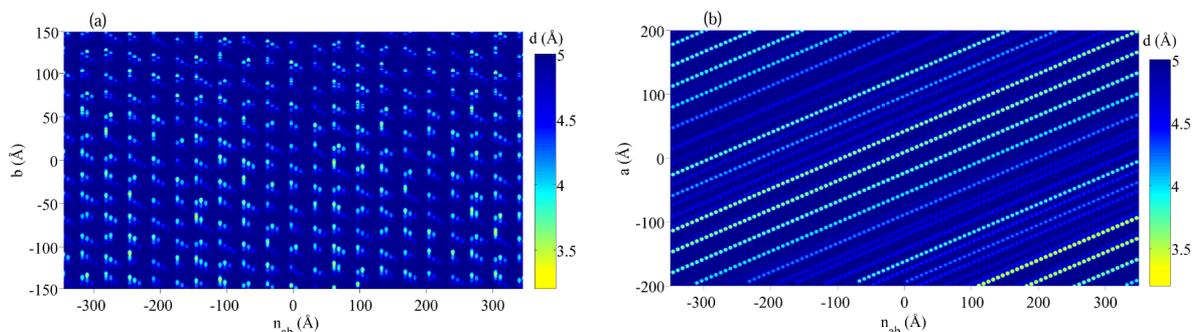

Figure 8. Spatial trapping pair distance distribution for a-boundary (a) and b-boundary (b) systems with the misorientation angle of 10°. The axis perpendicular to the ab plane is denoted as n_{ab}. Spatial trapping pair distance distribution is calculated using a radially symmetric weight function[53] calculated at the position of the molecular center of mass with a cutoff radius of 14.8 Å.
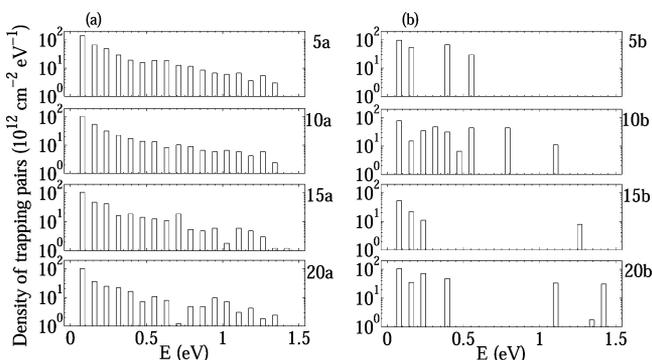
Figure 9. Electronic density of trap states at different grain boundaries. The boundaries are denoted as *Xy*, where *X* is the angle between monocrystal grains and *y* is the direction perpendicular to the boundary surface. Densities of trap states are given in a logarithmic scale. Energies of the trapping states are defined with the top of the valence band as a reference level.

grain boundary. For *b*-boundaries, the density of trap states is discrete with some distances preferred as a consequence of discrete density of trapping pairs at the grain boundary.

■ DISCUSSION

Our results clearly demonstrate the presence of trap states at the positions in the grain boundary where two molecules from opposite sides of the boundary are closely spaced, and hence, the electronic coupling of their HOMO orbitals is rather strong. In ref 23, it was argued that grain boundaries act as barriers for charge carriers rather than traps. Such an argument was drawn from an assumption that electronic coupling between molecules is weaker at the grain boundary than in the bulk. Our results show that such an assumption is not appropriate; strong electronic coupling at certain positions at the boundary creates trap states within the band gap of the material. However, one should also note that electronic coupling between neighboring molecules from opposite sides of the boundary can be weak at certain positions. At these positions, the grain boundary acts as a barrier and tends to confine the wave function to one side of the boundary. This effect can be seen from state (10) in Figure 3 and states (3) and (10) in Figure 4. Positions of strong electronic coupling and trap states will be absent only in the case of a grain boundary void when two grains with the same orientation are separated by empty space. Consequently, a void (microcrack) within an organic crystal[54] is expected to act as a barrier.

On the other hand, various numerical simulations of organic crystal FETs were based on a model that considers the transport at the boundary as a thermoionic jump over the barrier or tunneling through the barrier.[12,16,21,22] One should note that FETs typically operate at high charge densities. Therefore, the traps become filled with carriers, which, in turn, create an electrostatic potential that acts as a barrier for the transport of other charges. Such "trap charging induced barriers" should be distinguished from the barriers discussed in the previous paragraph.

Using the obtained results, the density of trap states for naphthalene polycrystals can be estimated. The calculated number of trap states per unit of boundary surface of two misoriented grains is 3×10^{13} cm^{-2} in the case of the misorientation angle of 5° and *a*-boundary, and takes similar values for other boundaries. Only trapping pairs with mutual

distances below 4 Å were considered in the calculation. In the work of Chwang and Frisbie,[9] the density of trap states was estimated from activation energies for charge transport in a single grain boundary FET based on sexithiophene. It was found that trap densities at acceptor-like levels take values from 7.0×10^{11} to 2.1×10^{13} cm^{-2}, depending on the grain boundary length and the angle of misorientation. Therefore, our results are of the same order of magnitude as the experimentally based estimate for the material belonging to the same class of materials as naphthalene.

Next, we estimate the number of grain boundary induced trap states per unit of volume and compare it to other relevant material parameters. The typical size of experimentally evidenced monocrystal grains[8,9,20,55] is of the order of 1 μm, which translates into volume trap density of $N_t = 9 \times 10^{17}$ cm^{-3} assuming grains of a cubical shape. On the other hand, the number of energy states per unit of volume in the valence band of a bulk naphthalene monocrystal is $N_v = 6.1 \times 10^{21}$ cm^{-3}. Although N_t is much lower than N_v, it can still be significant to affect the charge transport and optical properties of naphthalene. In ref 55, grain boundary defects were identified as the most pronounced and the most stable defects. The density of point bulk defects was (over)estimated[55] to be in the $N_p = 10^{14}-10^{16}$ cm^{-3} range. Because our calculated value of N_t is larger than N_p, our results confirm the conclusion that grain boundary defects are the most pronounced defects.[55] A compilation of the estimates of the density of trap states from FET characteristics was reported in ref 11. The estimated density of states at 0.2 eV above the valence band is in the range of $(0.7-3) \times 10^{19}$ cm^{-3} eV^{-1}, whereas at 0.3 eV above the valence band, it is in the $(1.5-4) \times 10^{18}$ cm^{-3} eV^{-1} range (see Figure 6 in ref 11). On the basis of these values, one can roughly estimate the density of trap states with energies higher than 0.2 eV above the valence band to be in the $(10^{17}-10^{18})$ cm^{-3} range, which is of the same order of magnitude as our calculated N_t.

Finally, we discuss the implications of our findings on properties of electronic and optoelectronic devices based on this class of materials. Since our results show that hole traps are located at the positions of strongest electronic coupling between orbitals of the two molecules from opposite sides of the boundary, one expects that there will be an electronic trap at the same position. We have verified this expectation by performing an explicit calculation of electron states at the boundary. As a consequence, traps at grain boundaries will not prevent radiative recombination of electrons and holes in LED devices or light absorption in the case of solar cells. Nevertheless, the traps will certainly broaden the absorption or emission spectrum of the material. Furthermore, the estimated number of traps per unit of volume is comparable to typical charge carrier densities in operating LED and solar cell devices. As a consequence, charge carrier transport will certainly be strongly affected by the traps. On the other hand, FETs typically operate at charge carrier densities much larger than the trap densities. As a consequence, the traps are filled with carriers and affect the charge carrier transport only through electrostatic barriers created by the trapped charges, as discussed previously.

■ CONCLUSIONS

In this paper, we have introduced the methodology for the calculation of electronic states at grain boundaries in small molecule based organic semiconductors. We focused our study

on low-angle grain boundaries, since our results indicated that they have lower energies than high-angle grain boundaries. The results indicate that grain boundaries introduce trap states within the band gap of the material. Wave functions of these states are localized on pairs of molecules from opposite sides of the boundary whose mutual distance is smaller than the distance between two adjacent molecules in a monocrystal. Strong electronic coupling between the orbitals of the two molecules is responsible for the creation of the trap state. While the naphthalene molecule was used in our study, we expect that the origin of trap states will be the same in any other small molecule based organic semiconductor since electronic coupling as a mechanism of trap state creation is present in any other material from this class.

The energy of the trap state was found to correlate to the distance between two molecules that create the trap. This correlation was then used to calculate the electronic density of trap states solely based on geometrical arrangement of molecules near the boundary. This approach was exploited to calculate the density of trap states for different boundaries and estimate the number of trap states per unit of volume in a real polycrystal. This number is significant and may consequently reduce the carrier mobility and deteriorate the performance of devices based on polycrystalline organic semiconductors.

■ AUTHOR INFORMATION

Corresponding Author
*E-mail: marko.mladenovic@ipb.ac.rs.

Notes
The authors declare no competing financial interest.

■ ACKNOWLEDGMENTS

■ REFERENCES

(1) Cheung, D. L.; Troisi, A. Modelling Charge Transport in Organic Semiconductors: From Quantum Dynamics to Soft Matter. *Phys. Chem. Chem. Phys.* **2008**, *10*, 5941−5952.

(2) Friend, R. H.; Gymer, R. W.; Holmes, A. B.; Burroughes, J. H.; Marks, R. N.; et al. Electroluminescence in Conjugated Polymers. *Nature* **1999**, *397*, 121−128.

(3) Burroughes, J. H.; Bradley, D. D. C.; Brown, A. R.; Marks, R. N.; Mackay, K.; Friend, R. H.; Burns, P. L.; Holmes, A. B. Light-Emitting Diodes Based on Conjugated Polymers. *Nature* **1990**, *347*, 539−541.

(4) Colvin, V. L.; Schlamp, M. C.; Alivisatos, A. P. Light-Emitting Diodes Made from Cadmium Selenide Nanocrystals and a Semiconducting Polymer. *Nature* **1994**, *370*, 354−357.

(5) Dodabalapur, A.; Torsi, L.; Katz, H. E. Organic Transistors: Two-Dimensional Transport and Improved Electrical Characeristics. *Science* **1995**, *268*, 270−271.

(6) Li, G.; Shrotriya, V.; Huang, J.; Yao, Y.; Moriarty, T.; Emery, K.; Yang, Y. High-Efficiency Solution Processable Polymer Photovoltaic Cells by Self-Organization of Polymer Blends. *Nat. Mater.* **2005**, *4*, 864.

(7) Fu, Y.-T.; Risko, C.; Bredás, J.-L. Intermixing at the Pentacene-Fullerene Bilayer Interface: A Molecular Dynamics Study. *Adv. Mater.* **2013**, *25*, 878−882.

(8) Kalihari, V.; Tadmor, E. B.; Haugstad, G.; Frisbie, C. D. Grain Orientation Mapping of Polycrystalline Organic Semiconductor Films by Transverse Shear Microscopy. *Adv. Mater.* **2008**, *20*, 4033−4039.

(9) Chwang, A. B.; Frisbie, C. D. Temperature and Gate Voltage Dependent Transport Across a Single Organic Semiconductor Grain Boundary. *J. Appl. Phys.* **2001**, *90*, 1342−1349.

(10) Chapman, B.; Checco, A.; Pindak, R.; Siegrist, T.; Kloc, C. Dislocations and Grain Boundaries in Semiconducting Rubrene Single-Crystals. *J. Cryst. Growth* **2006**, *290*, 479−484.

(11) Kalb, W. L.; Haas, S.; Krellner, C.; Mathis, T.; Batlogg, B. Trap Density of States in Small-Molecule Organic Semiconductors: A Quantitative Comparison of Thin-Film Transistors with Single Crystals. *Phys. Rev. B* **2010**, *81*, 155315.

(12) Horowitz, G.; Hajlaoui, M. E. Mobility in Polycrystalline Oligothiophene Field-Effect Transistors Dependent on Grain Size. *Adv. Mater.* **2000**, *12*, 1046−1050.

(13) Nelson, S. F.; Lin, Y.-Y.; Gundlach, D. J.; Jackson, T. N. Temperature-Independent Transport in High-Mobility Pentacene Transistors. *Appl. Phys. Lett.* **1998**, *72*, 1854−1856.

(14) Sakanoue, T.; Sirringhaus, H. Band-like Temperature Dependence of Mobility in a Solution-Processed Organic Semiconductor. *Nat. Mater.* **2010**, *9*, 736−740.

(15) Lee, S. S.; Kim, C. S.; Gomez, E. D.; Purushothaman, B.; Toney, M. F.; Wang, C.; Hexemer, A.; Anthony, J. E.; Loo, Y.-L. Controlling Nucleation and Crystallization in Solution-Processed Organic Semiconductors for Thin-Film Transistors. *Adv. Mater.* **2009**, *21*, 3605−3609.

(16) Chen, J.; Tee, C. K.; Shtein, M.; Anthony, J.; Martin, D. C. Grain-Boundary-Limited Charge Transport in Solution-Processed 6,13Bis(tri-isopropylsilylethynyl) Pentacene Thin Film Transistors. *J. Appl. Phys.* **2008**, *103*, 114513.

(17) Gundlach, D. J.; Royer, J. E.; Park, S. K.; Subramanian, S.; Jurchescu, O. D. Contact-Induced Crystallinity for High-Performance Soluble Acene-Based Transistors and Circuits. *Nat. Mater.* **2008**, *7*, 216−221.

(18) Rivnay, J.; Jimison, L. H.; Northrup, J. E.; Toney, M. F.; Noriega, R.; Lu, S.; Marks, T. J.; Facchetti, A.; Salleo, A. Large Modulation of Carrier Transport by Grain-Boundary Molecular Packing and Microstructure in Organic Thin Films. *Nat. Mater.* **2009**, *8*, 952−958.

(19) Dickey, K.; Anthony, J.; Loo, Y.-L. Improving Organic Thin-Film Transistor Performance through Solvent-Vapor Annealing of Solution-Processable Triethylsilylethynyl Anthradithiophene. *Adv. Mater.* **1976**, *21*, 392.

(20) Carlo, A. D.; Piacenza, F.; Bolognesi, A.; Stadlober, B.; Maresch, H. Influence of Grain Sizes on the Mobility of Organic Thin-Film Transistors. *Appl. Phys. Lett.* **2005**, *86*, 263501.

(21) Verlaak, S.; Arkhipov, V.; Heremans, P. Modeling of Transport in Polycrystalline Organic Semiconductor Films. *Appl. Phys. Lett.* **2003**, *82*, 745−747.

(22) Horowitz, G. Tunneling Current in Polycrystalline Organic Thin-Film Transistors. *Adv. Funct. Mater.* **2003**, *13*, 53−60.

(23) Kaake, L. G.; Barbara, P. F.; Zhu, X.-Y. Intrinsic Charge Trapping in Organic and Polymeric Semiconductors: A Physical Chemistry Perspective. *J. Phys. Chem. Lett.* **2010**, *1*, 628−635.

(24) Nan, G.; Li, Z. Modeling of Charge Transport in Polycrystalline Sexithiophene From Quantum Charge Transfer Rate Theory Beyond the First-Order Perturbation. *Org. Electron.* **2011**, *12*, 2198−2206.

(25) Verlaak, S.; Heremans, P. Molecular Micromolecular View on Electronic States Near Pentacene Grain Boundaries. *Phys. Rev. B* **2007**, *75*, 115127.

(26) Troisi, A.; Orlandi, G. Charge-Transport Regime of Crystalline Organic Semiconductors: Diffusion Limited by Thermal Off-Diagonal Electronic Disorder. *Phys. Rev. Lett.* **2006**, *96*, 086601.

(27) Nan, G.; Yang, X.; Wang, L.; Shuai, Z.; Zhao, Y. Nuclear Tunneling Effects of Charge Transport in Rubrene, Tetracene, and Pentacene. *Phys. Rev. B* **2009**, *79*, 115203.

(28) Shuai, Z.; Wang, L.; Li, Q. Evaluation of Charge Mobility in Organic Materials: From Localized to Delocalized Descriptions at a First-Principles Level. *Adv. Mater.* **2011**, *23*, 1145−1153.

(29) Sánchez-Carrera, R. S.; Atahan, S.; Schrier, J.; Aspuru-Guzik, A. Theoretical Characterization of the Air-Stable, High-Mobility Dinaphtho[2,3-b:2′ 3′-f]thieno[3,2-b]-thiophene Organic Semiconductor. *J. Phys. Chem. C* **2010**, *114*, 2334−2340.

(30) Hannewald, K.; Stojanović, V. M.; Schellekens, J. M. T.; Bobbert, P. A.; Kresse, G.; Hafner, J. Theory of Polaron Bandwidth Narrowing in Organic Molecular Crystals. *Phys. Rev. B* **2004**, *69*, 075211.

(31) Ortmann, F.; Bechstedt, F.; Hannewald, K. Theory of Charge Transport in Organic Crystals: Beyond Holstein's Small-Polaron Model. *Phys. Rev. B* **2009**, *79*, 235206.

(32) Martinelli, N. G.; Olivier, Y.; Athanasopoulos, S.; Delgado, M. C. R.; Pigg, K. R.; et al. Influence of Intermolecular Vibrations on the Electronic Coupling in Organic Semiconductors: The Case of Anthracene and Perfluoropentacene. *ChemPhysChem* **2009**, *10*, 2265−2273.

(33) Ciuchi, S.; Fratini, S. Electronic Transport and Quantum Localization Effects in Organic Semiconductors. *Phys. Rev. B* **2012**, *86*, 245201.

(34) Ciuchi, S.; Fratini, S.; Mayou, D. Transient Localization in Crystalline Organic Semiconductors. *Phys. Rev. B* **2011**, *83*, 081202.

(35) Ciuchi, S.; Fratini, S. Band Dispersion and Electronic Lifetimes in Crystalline Organic Semiconductors. *Phys. Rev. Lett.* **2011**, *106*, 166403.

(36) Perroni, C. A.; Marigliano Ramaglia, V.; Cataudella, V. Effects of Electron Coupling to Intramolecular and Intermolecular Vibrational Modes on the Transport Properties of Single-Crystal Organic Semiconductors. *Phys. Rev. B* **2011**, *84*, 014303.

(37) Vukmirović, N.; Bruder, C.; Stojanović, V. M. Electron-Phonon Coupling in Crystalline Organic Semiconductors: Microscopic Evidence for Nonpolaronic Charge Carriers. *Phys. Rev. Lett.* **2012**, *109*, 126407.

(38) Allen, M.; Tildesley, D. J. *Computer Simulation of Liquids*; Oxford University Press: New York, 1987.

(39) Parr, R. G.; Yang, W. *Density-Functional Theory of Atoms and Molecules*; Oxford University Press: New York, 1989.

(40) Vukmirović, N.; Wang, L. W. Charge Patching Method for Electronic Structure of Organic Systems. *J. Chem. Phys.* **2008**, *128*, 121102.

(41) Vukmirović, N.; Wang, L. W. Electronic Structure of Disordered Conjugated Polymers: Polythiophenes. *J. Phys. Chem. B* **2009**, *113*, 409−415.

(42) Martin, M. G.; Siepmann, J. I. Transferable Potentials for Phase Equilibria. 1. United-Atom Description of *n*-Alkanes. *J. Phys. Chem. B* **1998**, *102*, 2569−2577.

(43) Wick, C. D.; Martin, M. G.; Siepmann, J. I. Transferable Potentials for Phase Equilibria. 4. United-Atom Description of Linear and Branched Alkenes and Alkylbenzenes. *J. Phys Chem. B* **2000**, *104*, 8008−8016.

(44) Rai, N.; Bhatt, D.; Siepmann, J. I.; Fried, L. E. Monte Carlo Simulations of 1,3,5-Triamino-2,4,6-trinitrobenzene (TATB): Pressure and Temperature Effects for the Solid Phase and Vapor-Liquid Phase Equilibria. *J. Chem. Phys.* **2008**, *129*, 194510.

(45) Rai, N.; Siepmann, J. I. Transferable Potentials for Phase Equilibria. 10. Explicit-Hydrogen Description of Substituted Benzenes and Polycyclic Aromatic Compounds. *J. Phys. Chem. B* **2013**, *117*, 273−288.

(46) Sánchez-Carrera, R. S.; Paramonov, P.; Day, G. M.; Coropceanu, V.; Bredás, J.-L. Interaction of Charge Carriers with Lattice Vibrations in Oligoacene Crystals from Naphthalene to Pentacene. *J. Am. Chem. Soc.* **2010**, *132*, 14437−14446.

(47) Schwoerer, M.; Wolf, H. C. *Organic Molecular Solids*; WILEY-VCH Verlag: Wienheim, Germany, 2008.

(48) Hummer, K.; Ambrosch-Draxl, C. Electronic Properties of Oligoacenes from First Principles. *Phys. Rev. B* **2005**, *72*, 205205.

(49) Ponomarev, V. I.; Filipenko, O. S.; Atovmyan, L. O. Improving Organic Thin-Film Transistor Performance through Solvent-Vapor Annealing of Solution-Processable Triethylsilylethynyl Anthradithiophene. *Kristallografiya* **1976**, *21*, 392.

(50) Schmidt, M.; Kusche, R.; Kronmüller, W.; von Issendorff, B.; Haberland, H. Experimental Determination of the Melting Point and Heat Capacity for a Free Cluster of 139 Sodium Atoms. *Phys. Rev. Lett.* **1997**, *79*, 99−102.

(51) Lee, J. A.; Rösner, H.; Corrigan, J. F.; Huang, Y. Phase Transitions of Naphthalene and Its Derivatives Confined in Mesoporous Silicas. *J. Phys. Chem. C* **2011**, *115*, 4738−4748.

(52) Canning, A.; Wang, L. W.; Williamson, A.; Zunger, A. Parallel Empirical Pseudopotential Electronic Structure Calculations for Million Atom Systems. *J. Comput. Phys.* **2000**, *160*, 29−41.

(53) Stankovic, I.; Hess, S.; Kröger, M. Structural Changes and Viscoplastic Behavior of a Generic Embedded-Atom Model Metal in Steady Shear Flow. *Phys. Rev. E* **2004**, *69*, 021509.

(54) Chen, J.; Tee, C. K.; Yang, J.; Shaw, C.; Shtein, M.; Anthony, J.; Martin, D. C. Thermal and Mechanical Cracking in Bis(triisopropyl-silylethynyl) Pentacene Thin Films. *J. Polym. Sci., Part B: Polym. Phys.* **2006**, *44*, 3631−3641.

(55) Verlaak, S.; Rolin, C.; Heremans, P. Microscopic Description of Elementary Growth Processes and Classification of Structural Defects in Pentacene Thin Films. *J. Phys. Chem. B* **2007**, *111*, 139−150.

(56) This work makes use of results produced by the High-Performance Computing Infrastructure for South East Europe's Research Communities (HP-SEE), a project co-funded by the European Commission (under contract number 261499) through the Seventh Framework Programme. HP-SEE involves and addresses specific needs of a number of new multi-disciplinary international scientific communities and thus stimulates the use and expansion of the emerging new regional HPC infrastructure and its services. Full information is available at: http://www.hp-see.eu/.

15748

dx.doi.org/10.1021/jp404825h | *J. Phys. Chem. C* 2013, 117, 15741−15748